# We are IntechOpen, the world's leading publisher of Open Access books Built by scientists, for scientists

**6,900**
Open access books available

**186,000**
International authors and editors

**200M**
Downloads

Our authors are among the

**154**
Countries delivered to

**TOP 1%**
most cited scientists

**12.2%**
Contributors from top 500 universities

CLARIVATE ANALYTICS
**BOOK CITATION INDEX**
INDEXED

**WEB OF SCIENCE**™

Selection of our books indexed in the Book Citation Index
in Web of Science™ Core Collection (BKCI)

## Interested in publishing with us?
### Contact book.department@intechopen.com

Numbers displayed above are based on latest data collected.
For more information visit www.intechopen.com

# Impact of Solar Radiation Data and Its Absorption Schemes on Ocean Model Simulations

Goro Yamanaka, Hiroshi Ishizaki, Hiroyuki Tsujino,
Hideyuki Nakano and Mikitoshi Hirabara
*Meteorological Research Institute, Japan Meteorological Agency*
*Japan*

## 1. Introduction

Since absorption of solar radiation plays a major role in heating the upper ocean layers, it is essential for modeling physical, chemical and biological processes (e.g., ocean general circulation or marine carbon cycle). In order to simulate the upper ocean thermal structures as realistically as possible, an ocean general circulation model (OGCM) requires accurate solar radiation data, used as the surface boundary condition. In this sense, it is important to recognize the quality of the solar radiation data being expected or suitable for OGCMs beforehand. The appropriate choice of absorption schemes of solar radiation is also important for ocean modeling in the upper ocean. The absorption of solar radiation is greatly affected by many factors, such as the wavelength of sunlight, the zenith angle and ocean optical properties in the ocean interior. Many absorption schemes have attempted to mimic these processes, but the impact of those schemes on the upper ocean thermal structures is not yet fully understood.

The aim of this study is to determine the importance of solar radiation in ocean modeling. In particular, we examine the impact of both prescribed solar radiation data and its absorption schemes on OGCM simulations. The knowledge obtained here is expected to be useful for ocean modeling studies, as well as for understanding the upper ocean thermal structure.

This article is organized as follows. Section 2 examines the impact of solar radiation flux on ocean model simulation, focusing on discrepancies between simulated and observed sea surface temperature (SST) variations. Yamanaka (2008) discussed such discrepancies over the tropical Indian Ocean, whereas this study deals extensively with discrepancies over the tropical Indo-Pacific Ocean. Section 3 introduces three types of absorption schemes in solar radiation into an ocean model and examines the impact of those schemes on ocean model simulation. Section 4 summarizes this study.

## 2. Impact of incident solar radiation data on an ocean model simulation

### 2.1 Brief introduction

Indian Ocean SSTs have notably increased since the late 20th century (Lau & Weng, 1999). Figure 1 clearly shows that the positive SST anomaly has dominated especially after the mid-1980s.
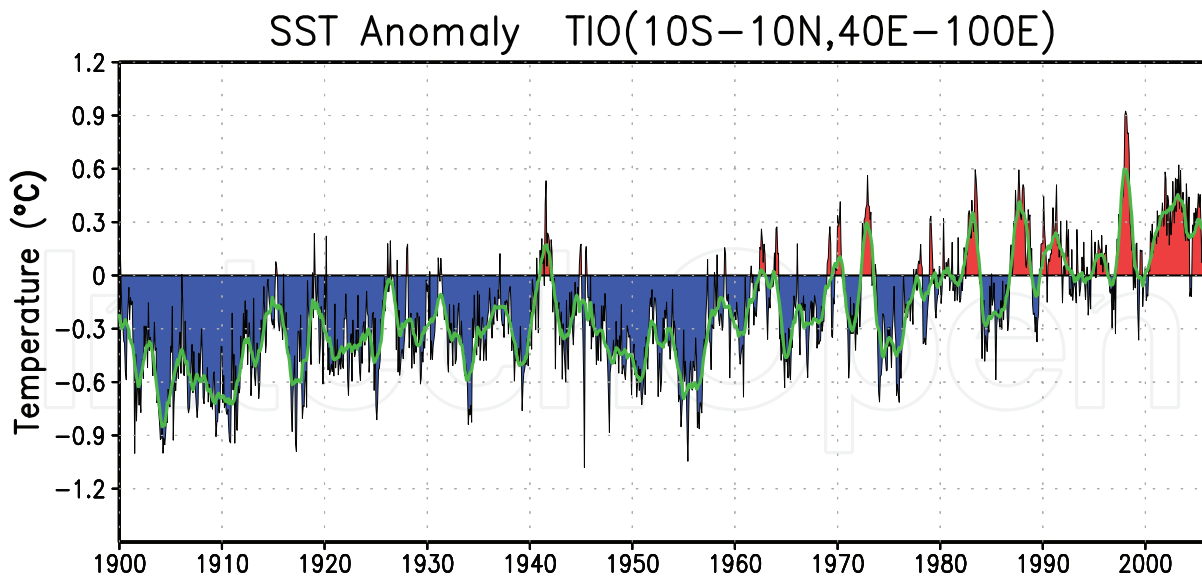
Fig. 1. Time series of the SST anomaly [°C] averaged in the tropical Indian Ocean (10°S-10°N, 40°E-100°E). The SST data set is based on COBE-SST (Ishii et al., 2005). The red (blue) shaded area denotes positive (negative) anomalies. The base period is from 1971 to 2000.

The warming of the tropical Indian Ocean is likely caused by climate variations, but may also, in turn, trigger some impacts on surrounding regions. Some studies using an atmospheric general circulation model (AGCM) with the prescribed SST suggest that the increasing trend in Indian Ocean SSTs can impact the climate. For example, Hoerling et al. (2004) indicated that local increases in precipitation associated with the warming of the Indian Ocean resulted in a remote response to the mid and high latitudes through the release of latent heat, and contributed to an increased trend of the North Atlantic Oscillation (NAO). Also, the warming of the Indian Ocean enhances the anti-cyclonic circulation anomaly at the lower level of the troposphere over the Philippines during the mature phase of El Nino (Watanabe & Jin, 2002), which has a major impact on the East Asian climate (Wang et al., 2000).

In order to understand the warming mechanism of the Indian Ocean, it is necessary to clarify the observation-based surface heat balance over the Indian Ocean. However, due to lack of long-term observation, many studies used OGCMs to diagnose the surface heat balance (e.g., Du et al., 2005; Murtugudde and Busalacchi, 1999).

The importance of the OGCM study is to know to what extent variations of the Indian Ocean are simulated by the model. Figures 2a and 2d show the anomaly correlation between observed and simulated SSTs, which is one of the means by which the model's performance may be determined. It is found that the anomaly correlation over the tropical Indian Ocean is below 0.6 and is less than that in other areas, such as the tropical Pacific and the mid and high latitudes. Poor simulation of the tropical Indian Ocean makes it difficult to analyze the surface heat balance over that area. However, the cause of this poor simulation is not yet fully understood.

This section aims to investigate the cause of the poor simulation, basically following Yamanaka (2008) and extensively looking at the tropical Indo-Pacific Ocean.
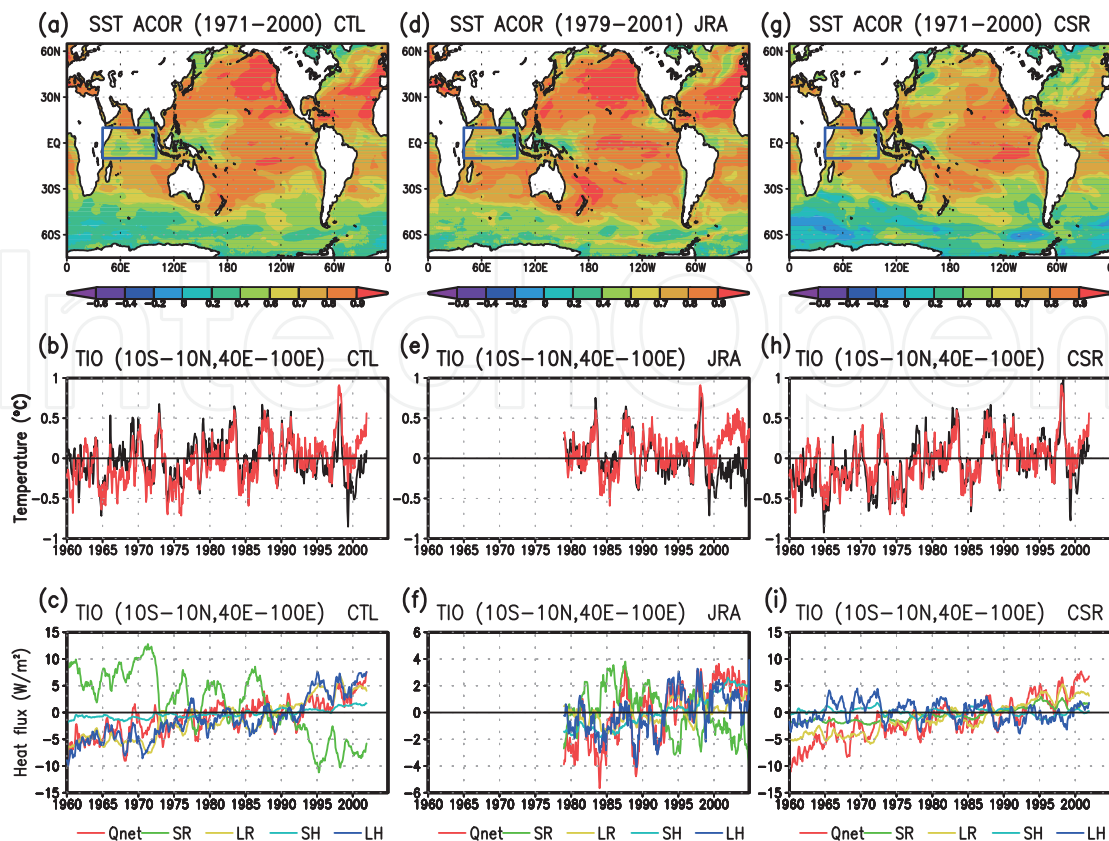
Fig. 2. (a) Annual mean anomaly correlation between the observed and the simulated SST anomalies for CTL. The statistical period is from 1971 to 2000. (b) Time series of the observed (red) and simulated (black) SST anomalies [°C] averaged in the tropical Indian Ocean (10°S-10°N, 40°E-100°E) for CTL. The base period is from 1971 to 2000. (c) Time series of sea surface heat flux anomalies [W m$^{-2}$] averaged in the tropical Indian Ocean (10°S-10°N, 40°E-100°E) for CTL. Lines denote net surface heat flux (red), solar radiation (green), long wave radiation (yellow), sensible heat flux (aqua), and latent heat flux (blue). The base period is from 1971 to 2000. (d)-(f) Same as (a)-(c) but for JRA. The base period is from 1979 to 2004. (g)-(i) Same as (a)-(c) but for CSR.

## 2.2 Model and methodology

We used a version of the Meteorological Research Institute community ocean model (MRI.COM) (Ishikawa et al., 2005), which is a z-coordinate primitive-equation model. The model domain is near global, from 75°S to 75°N. The horizontal resolution is 1° in longitude and 1° in latitude (0.3° near equator). The model has 50 vertical levels, with 24 levels in the top 200m.

Two sets of daily atmospheric reanalysis data are used as the surface boundary condition: ECMWF 40-year reanalysis data (hereafter ERA-40) (Uppala et al., 2005) from 1960 to 2001, and Japan Meteorological Agency 25-year reanalysis data (hereafter JRA-25) (Onogi et al., 2007) from 1979 to 2004. We used the bulk formula for the surface fluxes by Kara et al. (2000). After the model was integrated for 102 years as spin-up, three experiments were conducted with different interannual atmospheric forcing data. In CTL, the model was driven by atmospheric variables derived from ERA-40; in JRA, the model was driven by those

derived from JRA-25. In CSR, the atmospheric forcing was the same as that in CTL, except that solar radiation data included only seasonal variations (no interannual or longer variations).

For comparison, we used the COBE-SST data set of in-situ measurements of SST (Ishii et al., 2005). The reanalyzed solar radiation data derived from ERA-40 and JRA-25 reanalysis were compared with satellite-based estimates of solar radiation: International Satellite Cloud Climatology Project (ISCCP) solar radiation data derived from the Common Ocean-ice Reference Experiment (hereafter CORE/ISCCP) (Large & Yeager, 2004). Also, the reanalyzed precipitation data derived from ERA-40 and JRA-25 were compared with two observation-based estimates of precipitation: Climate Prediction Center (CPC) Merged Analysis of Precipitation combined with NCEP/NCAR R1 reanalysis (hereafter CMAP) (Xie & Arkin, 1996), and Global Precipitation Climate Project Version 2 (hereafter GPCP) (Adler et al., 2003).

All data was converted to monthly means before further analysis. Monthly mean data for ERA-40 surface flux was produced using the daily mean data based on 36 hour forecast data at each 12UTC initials.

## 2.3 Results

### 2.3.1 The simulated Indian Ocean with the prescribed solar radiation

Figure 2b shows the time evolution of simulated SST anomalies over the tropical Indian Ocean (10°S-10°N, 40°E-100°E) for CTL. The model was successful in simulating the interannual SST variation of 4 to 5 years associated with ENSO, but failed to capture the long-term warming trend found in the observed SSTs. For example, the simulated SST anomaly was slightly higher than the observed one in the 1960s, whereas it was substantially lower than observed after the late 1990s, indicating a cooling bias. A similar tendency was also found in JRA (Fig. 2e), where the simulated SST anomaly in the Indian Ocean has been gradually cooler than the observed one since the late 1980s, and the difference has increased since 2000. This result implies that the poor simulation of the Indian Ocean SSTs in both experiments is due to the cooling bias, especially in the late 1990s.

Cooling of the model Indian Ocean after 1990 was observed not only at the surface, but also below the surface. Figure 3a shows the mixed layer change between 10 years in CTL. The deepening of the mixed layer depth (MLD) was found to be wide in the tropical Indian Ocean. Figures 3b and 3c show vertical profiles of temperature and potential density at the equatorial Indian Ocean (EQ, 90°E) between January 1990 and January 2000 in CTL. Temperature decreased up to about 60 m depth, and the MLD increased to 100 m depth during that ten-year period. This simulated cooling trend in the upper ocean differs from the trend observed by Levitus et al. (2005), in which significant warming near the surface accompanied cooling in the upper thermocline (Han et al., 2006). The deepening of the mixed layer may have altered the surface heat balance of the Indian Ocean in the model.

Next, we examine surface fluxes used as the surface forcing for the model. Figure 2c shows the time duration of each component (net flux, solar radiation, long wave radiation, sensible heat flux, and latent heat flux) of the model surface flux anomalies. It is noted that the solar radiation anomaly (green line) in CTL exhibits a significant decreasing trend. From the 1960s to early 1970s, the solar radiation anomaly was positive, corresponding to the simulated warmer SST anomaly. After the mid-1990s, the negative solar radiation anomaly became
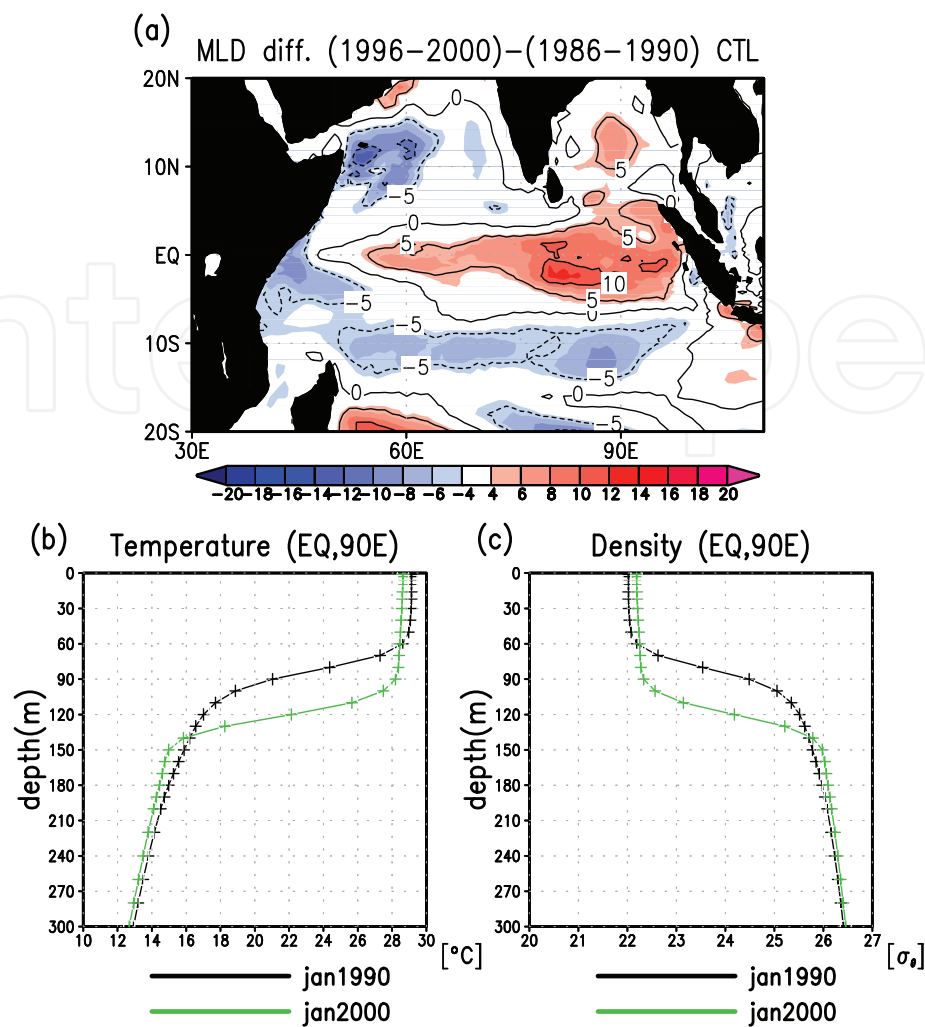
Fig. 3. (a) Mixed layer depth difference [m] between the 1996-2000 mean and the 1986-1990 mean. The shaded area denotes where the difference is positive. (b) Vertical profile of temperature [°C] in the equatorial Indian Ocean in CTL on January 1990 (black) and on January 2000 (green). (c) Same as (b) but for potential density [$\sigma_\theta$].

dominant, corresponding to the cold bias of the model in this period. Sensible and latent heat fluxes partly weakened the decreasing trend caused by solar radiation because they were restored to the observed atmospheric variables based on the bulk formula. However, a decreasing trend remained in the simulated SSTs. A similar decreasing trend in the solar radiation anomaly was also found in JRA (Fig. 2f).

In order to clarify the role of the reanalyzed solar radiation data on the cooling bias in the simulated SSTs, an additional experiment (CSR) was carried out, where the atmospheric forcing was the same as at CTL except that the daily-mean climatological solar radiation data was used. Figure 2h shows that the simulated SSTs in CSR agree better with the observed SSTs (e.g., improvement in both the warming bias in the 1960s and the cooling bias in the late 1990s, compared to those in CTL). Also, the warming of the Indian Ocean in the 1990s was roughly captured in CSR even under climatological solar radiation forcing. According to the sea surface flux anomalies (Fig. 2i), the variability of the net heat flux was controlled by long wave radiation on a longer time scale, as well as by latent heat flux on an interannual time

scale. These results suggested that increases in downward long wave radiation contributed to the simulated warming of the Indian Ocean in the 1990s in CSR.

Improvement of the bias in the simulated SSTs of the Indian Ocean was expected to result in better performance of the simulated SSTs. Figure 2g shows the annual mean anomaly correlation between the observed and the simulated SST anomalies in CSR. It was found that removal of the variations of the reanalyzed solar radiation on an interannual or longer timescale improved the simulated SST variability, especially in the tropical Indian Ocean. The SST skill increased by 0.1 to 0.3 in this region, compared to that of CTL. In the central to eastern equatorial Pacific, however, no significant change in SST variability was observed between CTL and CSR. It is suggested that the SST variability in the central to eastern equatorial Pacific is determined mainly by wind stress, rather than solar radiation. However, in the mid and high latitudes, the SST skill is significantly reduced in CSR, implying that SST variability in these regions is determined by variation in solar radiation.

These results strongly suggest that the cooling of simulated Indian Ocean SSTs is primarily caused by the atmospheric reanalysis data used as the surface boundary condition. Next, we examine why the atmospheric reanalysis products display decreasing trends in solar radiation.
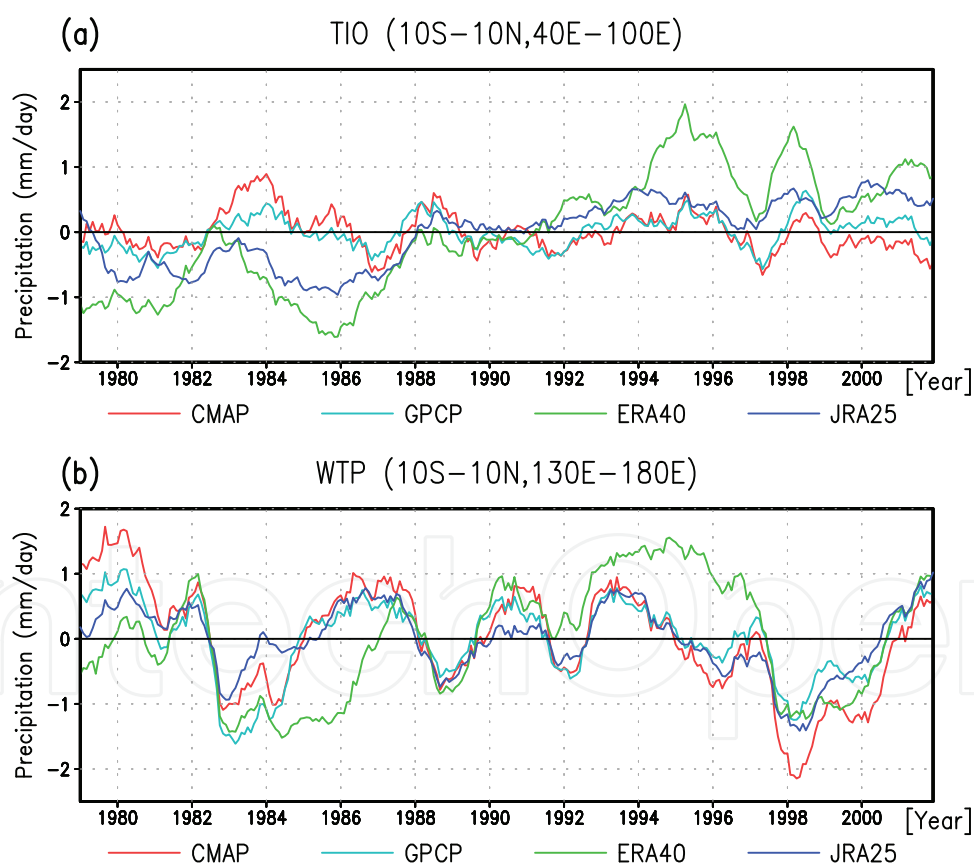


Fig. 4. Time series of 13-month running mean precipitation anomalies [mm/day] averaged over (a) the tropical Indian Ocean (10°S-10°N, 40°E-100°E) and (b) the western tropical Pacific (10°S-10°N, 130°E-180°) for CMAP (red), GPCP (acua), ERA-40 (green), and JRA-25 (blue).

### 2.3.2 Spurious trends included in atmospheric reanalysis data

Figure 4 shows a time series of precipitation anomalies averaged over the tropical Indian Ocean and the western tropical Pacific, based on the reanalysis data with the CMAP and GPCP data sets as reference. Over the tropical Indian Ocean, ERA-40 precipitation (green line) is generally greater than the observed precipitation, and an increasing trend is clearly seen since 1979. JRA-25 precipitation (blue line) also exhibits a similar increasing trend, though not as great as that of the ERA-40 precipitation. On the other hand, the observed precipitations in CMAP and GPCP exhibit no significant increasing trend, and also may be the observed cloud amount. In contrast, over the western tropical Pacific, the observed precipitation and the JRA-25 precipitations show a slight decreasing trend, though the ERA-40 precipitation indicates no significant trend.
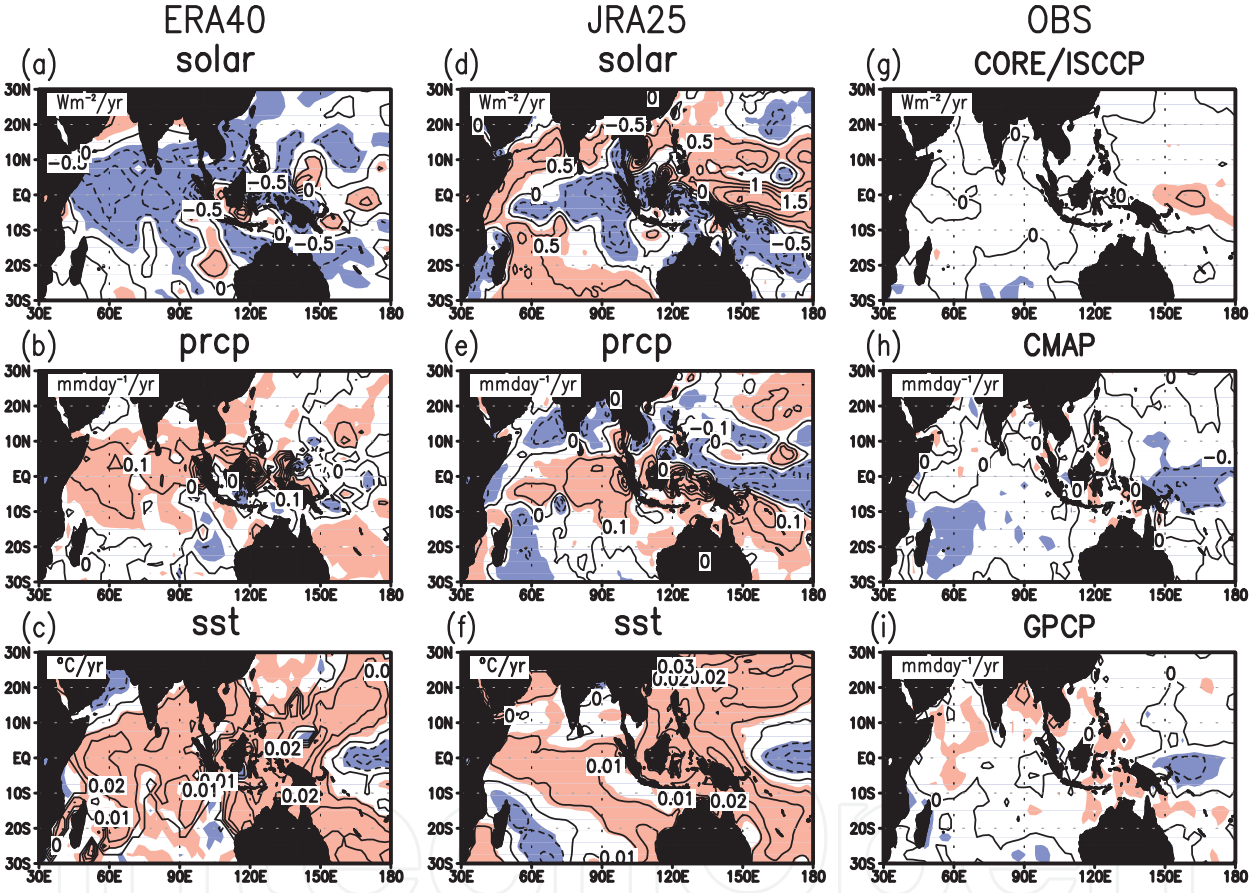


Fig. 5. Average trends from 1979 to 2001 in the reanalysis products (ERA-40 and JRA-25) and observed data (CORE/ISCCP, CMAP and GPCP) for solar radiation (upper), precipitation (middle), and the prescribed SST for the reanalyses (lower) over the Indian Ocean. The contour interval is $0.5\,\mathrm{Wm^{-2}}$/year for solar radiation, $0.1\,\mathrm{mm\,day^{-1}}$/year for precipitation, and $0.01\,^{\circ}\mathrm{C}$/year for SST. The red (blue) shaded areas denote where the rate of change is positive (negative) with statistical significance.

Figure 5 shows average trends during the period 1979 to 2001 in the atmospheric reanalysis products (ERA-40 and JRA-25) with the prescribed SSTs for the reanalyses, in addition to CORE/ISCCP solar radiation and CMAP precipitation. Over the tropical Indian Ocean, the

reanalysis products exhibit decreasing trends in solar radiation, and their spatial patterns are almost the reverse of the precipitation patterns. This feature is generally found in all the reanalysis products, though it seems more pronounced in JRA-25 and ERA-40 than in NCEP/NCAR 40-year reanalysis (Kalnay et al., 1996) and NCEP-DOE AMIP-II reanalysis (Kanamitsu et al., 2002) as described in Yamanaka (2008). The increasing trend in precipitation roughly corresponds to the increasing trend in SSTs prescribed as the lower boundary condition for the reanalyses. Hence, the decrease in solar radiation may be associated with increase in precipitation directly over the region of the most rapidly warming SST. In contrast, no increasing trend in solar radiation over the Indian Ocean was observed in the CORE/ISCCP data. Also, the CMAP data showed no increasing trend in precipitation nor a decreasing trend over the southern Indian Ocean. Over the western tropical Pacific, the situation was almost the same; the area with a slightly decreasing trend in precipitation or a slightly increasing trend in solar radiation corresponds to the cooling SST region, suggesting a linkage between the trends in atmospheric reanalysis and the SST.

Several problems in the atmospheric reanalyses may have caused this spurious increasing trend in precipitation over the tropical Indian Ocean. One problem may arise from bias in the assimilation, for example, ERA-40 has rainfall problems over tropical oceans from the early 1990s, associated with the bias of satellite radiance corrupted by the Pinatubo eruption (Dee et al., 2008), and JRA-25 has major discontinuous changes associated with transition from TOVS to ATOVS in November 1998 (Tsutsui & Kadokura, 2008). Another problem may come from the bias in the model. Over the tropical oceans, where in-situ observations are infrequent and sparse, a reanalysis dataset would be equivalent to AGCM outputs where SST is given as the lower boundary condition (Arakawa & Kitoh, 2004). Hence, responding to the warming of the Indian Ocean, AGCM tends to enhance convective activities and thus to increase precipitation and cloud amounts.

As a result, the decrease in the solar radiation caused a cooling trend of the simulated SSTs in the Indian Ocean, which is inconsistent with the observed SSTs (Fig. 1). This is supported by the fact that the area with a relatively low skill of simulated SSTs in the tropical Indian Ocean approximately corresponds to that with a decreasing trend in solar radiation (Fig. 2a).

### 2.3.3 Discussion

We found that the poor simulation of the Indian Ocean SST was due to the atmospheric reanalysis data (ERA-40 and JRA-25) used as the surface boundary condition for OGCM, which included decreasing trends in solar radiation there. This decreasing trend in solar radiation was related to the increasing trend in precipitation over the Indian Ocean, which was partially as a response to the local warming of the SSTs.

The spurious trends in the atmospheric reanalysis products constitute a crucial problem for long-term ocean modeling studies, because surface flux data based on the atmospheric reanalysis products are widely used as the surface boundary conditions for OGCMs. Thus, caution is necessary when using atmospheric reanalysis data as the surface boundary conditions for OGCMs. One approach to avoid the unrealistic cooling of the model Indian Ocean is to use the CORE/ISCCP solar radiation. The CORE/ISCCP solar radiation data do not exhibit significant decreasing trend over the tropical Indian Ocean (Fig. 5), although it should be noted that the CORE/ISCCP solar radiation data included no interannual variations before mid-1983, because of the limited availability of satellite data. In fact, a recent study

demonstrated that the ocean model driven by the CORE forcing (Large & Yeager, 2009) reasonably simulated long-term variations in the tropical Indian Ocean (Tsujino et al., 2011).

Several studies suggest that there may be no increase or even decrease in precipitation over the Indian Ocean. Copsey et al. (2006) reported a rise in sea surface pressure, as a proxy for precipitation, over the Indian Ocean between 1950 and 1996. Deser & Phillips (2006) concluded that there was no significant increase in precipitation over the Indian Ocean, based on analysis of the cloud amount and wind convergence over the ocean. Norris (2005) suggested a negative trend in upper level cloud cover in the equatorial Indian Ocean between 1952 and 1997. Further study based on observation is needed to clarify the long-term trend of precipitation in the Indian Ocean.

## 3. Impact of absorption schemes in solar radiation on an ocean model simulation

### 3.1 Brief introduction

The optical properties of seawater, which dominate the distribution of the penetration and absorption of the given outer radiation, are primarily determined by the phytoplankton biomass, measured by chlorophyll-a concentration in seawater, with their accompanying retinue of dissolved and particulate materials of biological origin (Case 1 Waters) (e.g., Morel, 1988; Morel & Prieur, 1977). Many studies have focused on the development of shortwave penetration schemes including the effects of chlorophyll-a concentration either in bulk or spectral formulae (e.g., Manizza et al., 2005; Morel, 1988; Morel & Antoine, 1994; Ohlmann, 2003; Ohlmann et al., 2000; Ohlmann & Siegel, 2000) and on the effects of these parameterizations on the ocean dynamics and thermodynamics through forced ocean model experiments (e.g., Anderson et al., 2007; Manizza et al., 2005; Murtugudde et al., 2002; Nakamoto et al., 2001). While the direct effect of including the chlorophyll-a concentration increased absorption in shallower layers, one of the most pronounced changes was the indirect effect: an increased cooling in SST in the eastern equatorial Pacific. This increased cooling resulted from increased upwelling through changes in the equatorial current system (Gnanadesikan & Anderson, 2009; Manizza et al., 2005; Murtugudde et al., 2002; Nakamoto et al., 2001; Sweeney et al., 2005).

The solar zenith angle or the solar altitude affects penetrating radiation and the vertical distribution of heating by absorbing the radiation in a water column under clear sky condition. Some shortwave penetration schemes explicitly examined the effects of solar altitude on this (e.g., Morel & Antoine, 1994; Ohlmann, 2003). Ishizaki & Yamanaka (2010) (hereafter referred to as IY10) examined the impact of sun altitude on ocean radiant heating, assuming that all sunlight is direct solar rays. They introduced sun altitude into the simple radiation formulation of Paulson & Simpson (1977) (hereafter referred to as PS77) with diurnal changing incident angle, and studied the sensitivity of an ocean model to the formulation. Introduction of the solar angle caused the effective attenuation depth for the diurnal-mean penetrating radiation shallower than that of the downward vertical radiation, and caused the locus of radiation absorption to shift upward. This was qualitatively the same as including chlorophyll-a concentration, resulting in the same indirect effect of cooling in SST in the eastern equatorial Pacific.

Here we examined the impact of solar radiation absorption schemes on ocean model simulation. We considered three absorption schemes. The first is a conventional scheme based on PS77, in which sunlight has diurnal constant intensity and is vertically downward.

The second is the above-mentioned IY10 scheme, in which sunlight has a diurnal changing incident angle, leading to vertical change in the diurnal-mean attenuation rate of the sun light. The third scheme introduces the effect of chlorophyll-a concentration by Morel & Antoine (1994)'s (hereafter referred to as MA94) formulation, in addition to the second scheme. We confirmed the impact of these three schemes on the mean ocean state, especially focusing on the effective euphotic layer depth, temperature and current fields.

### 3.2 Formulations of three absorption schemes

### 3.2.1 Basic assumption

We made the following assumptions for formulating the changing solar altitude angle of the sun: (a) All sunlight consists solely the direct rays without any scattered light. (b) The sun is a point source of light, i.e., the visual angle of the sun is zero. (c) The ratio of the actual to the mean earth-sun separation is assumed to be unity, that is, the earth's revolution orbit is perfectly circular. (d) The declination angle, $\delta$, of the sun (i.e., its latitude on the celestial sphere) is constant on a diurnal time scale. (e) The effective radiation intensity $I_{org}$ of sunlight on a plane perpendicular to the ray is diurnal constant, regardless of the sun altitude, and is calculated from the diurnal-mean irradiance $I_{DM}$ given as a boundary condition (IY10). (f) The refractive index of seawater $\gamma$ is a constant, i.e., $\gamma = 1.34$. (g) The optical characteristics of seawater are homogeneous with depth, in horizontal direction, and over time, and are assumed to be of Jerlov (1968) Water Type I (PS77) for the first (PS77) and the second (IY10) absorption scheme. This water has an e-folding depth (attenuation depth) of 23 m for the shorter wavelength part (PS77). (h) Sea surface albedo $\alpha$ is set to be a constant, 0.066, independent of sun altitude.

### 3.2.2 Formulation

According to PS77, incoming solar radiation is divided into two parts: the longer-wavelength (infrared (IR)), which is absorbed immediately at the sea surface and the shorter-wavelength (visible plus ultra-violet (visible-UV)), which penetrates a relatively long distance, which is expressed as

$$I/I_0 = R exp(-z/\zeta_1) + (1-R)exp(-z/\zeta_2) \tag{1}$$

where $I_0$ and $I$ are the irradiances just under the sea surface and at depth z, respectively; $R$ is the ratio of the IR part to the total at the surface; and $\zeta_1$ and $\zeta_2$ are the e-folding depths (attenuation depths) of the IR and visible-UV parts, respectively. We take this formulation as our first absorption scheme with $R = 0.58$, $\zeta_1 = 0.35$ m, and $\zeta_2 = 23$ m (for Water Type I) (PS77) and call it the "PS77-scheme".

For the second absorption scheme, the incoming radiation with incident angle $A$ at the sea surface penetrates the sea with refracted angle $A'$. The sun altitude $A$ is given by the observer's latitude $\theta$, declination of the sun $\delta$ ($-23.5° < \delta < 23.5°$), and the local time $t$ as

$$sinA = sin\delta sin\theta - cos\delta cos\theta cos\omega t \tag{2}$$

where $\omega$ is the diurnal angular velocity of the sun for the observer, i.e., $\omega = 2\pi/24$ hours. The relationship between $A$ and $A'$ is given by Snell's law:

$$cosA/cosA' = \gamma(= 1.34) \tag{3}$$

so that

$$sin A' = ((\gamma^2 - 1) + sin^2 A)^{1/2}/\gamma \tag{4}$$

The minimum of $A'$ is 41.7° for $A = 0°$. The path length is expressed as $z/sin A'$ where $z$ is the depth, so that

$$I/I_o = R exp(-z/(\zeta_1 sin A')) + (1 - R)exp(-z/(\zeta_2 sin A')) \tag{5}$$

where the values of $R$, $\zeta_1$, and $\zeta_2$ are the same as those of the first scheme. We call this the "IY10-scheme". The practical calculation procedure of solar radiation from a given diurnal-mean irradiance $I_{DM}$ is given in IY10.

For the third absorption scheme, MA94's formulation is used with a climatological chlorophyll-a data at 1 m depth. Chlorophyll-a data is derived from a Sea-viewing Wide Field-of-view Sensor (SeaWiFS; http://oceancolor.gsfc.nasa.gov/SeaWiFS). Their formulation is expressed as

$$I/I_o = F_{IR}exp(-z/(Z_{IR}sin A')) + F_{VIS}(V_1 exp(-z/Z_1) + V_2 exp(-z/Z_2)) \tag{6}$$

where $F_{IR}$ is the fraction of the infrared (IR) radiation (wavelengths $> 0.75\mu m$) to the total, $F_{VIS}$ is that for the visible- UV radiation ($F_{IR} + F_{VIS} = 1$), and $Z_{IR} = 0.267$ m, is the attenuation length of the IR radiation. The visible-UV part consists of two exponentials with the partitioning factors and attenuation depths, $V_1$, $V_2$ ($V_1 + V_2 = 1$), $Z_1$, and $Z_2$, depending on the chlorophyll-a concentration $C$. Here, the term including $Z_1$ in (6) represents the longer wavelength range of the visible-UV part, with $Z_1$ being of a few meters over the whole range of the chlorophyll-a concentration. They are expressed by polynomials of $log_{10}C$, and values of their coefficients and the functional forms of the four parameters are given for the range of $C$ between 0.02 and 20 mg m$^{-3}$ in MA94. Two sets of coefficients of the polynomials are given, one for uniform pigment profiles and the other for nonuniform ones. Here we use (6) with the variable solar incident angle even for the visible-UV part:

$$I/I_o = F_{IR}exp(-z/(Z_{IR}sin A')) + F_{VIS}(V_1 exp(-z/(Z_1 sin A')) + V_2 exp(-z/(Z_2 sin A'))) \tag{7}$$

The value of $F_{VIS}$ depends on the atmospheric condition and the solar zenith angle; MA94 gives the values 0.54 - 0.57 for clear skies and 0.60 for overcast skies. Here, however, we use $F_{VIS} = 1 - R$ ($F_{IR} = R = 0.58$) for the sake of consistency with the first and second absorption scheme. The polynomials for non-uniform pigment profiles are used because we used the chlorophyll-a data obtained by satellites (Morel & Berthon, 1989). We call this a modified MA94-scheme, that is, the "mMA94-scheme".

### 3.3 General features of optical property of sea surface layer

Before describing the implementation of the above schemes in an ocean model, we theoretically discuss the annual-mean of the diurnal-mean euphotic layer depth, attenuation depth (e-folding depth), and absorption of the penetrating radiation (only for the visible-UV part). To calculate the diurnal-mean radiation, the time step was taken as 1 min with the incident angle ($sin A$) calculated by (2) at every time step. Here, the radiation intensity of sunlight is assumed to be the solar constant 1.37 kW m$^{-2}$ only in this subsection and the sea surface irradiance $I_o$ is the intensity multiplied by $sin A$.
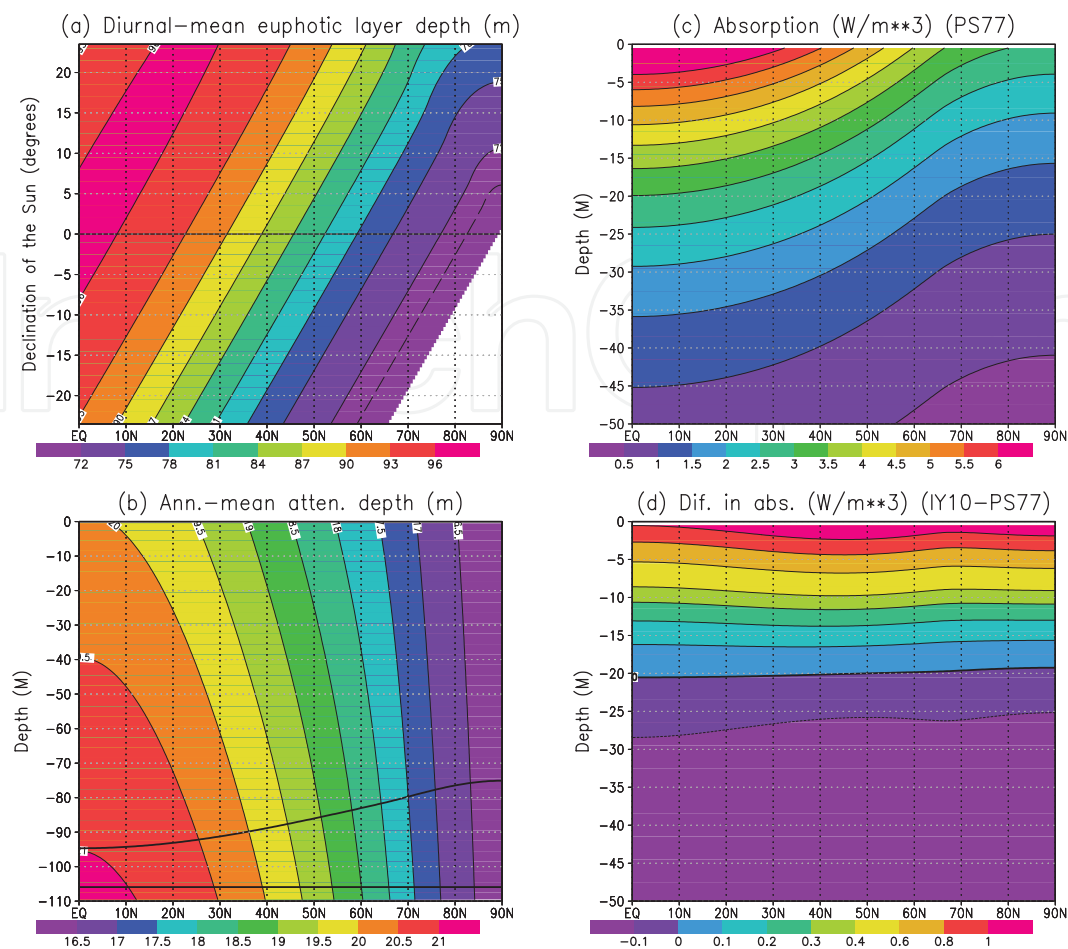
Fig. 6. (a) Diurnal-mean euphotic layer depth $d_e$ [m] for IY10, for the sun declination $\delta$ and the northern latitude $\theta$. (b) Meridional section of the effective attenuation depth $\zeta$ [m] defined in each 1 m-layer for annually averaged diurnal-mean penetrating irradiance of IY10. (c) Absorption of annually averaged irradiance of PS77 [W m$^{-3}$]. (d) Difference in absorption between IY10 and PS77 [W m$^{-3}$] (IY10 - PS77). The thick lines in (b) indicate the annual mean euphotic layer depth for IY10 and PS77 (constantly 105.9 m).

### 3.3.1 Difference between IY10 and PS77 schemes

The diurnal-mean euphotic layer depth $d_e$ for the IY10-scheme is a function of $\theta$ and $\delta$ (Fig. 6a), which was numerically obtained as the depth where diurnal-mean irradiance of the visible-UV part of the incident radiation became 1 % of its surface value. Depth $d_e$ ranged from less than 71 m in winter at high latitudes to more than 96 m at equatorial equinox through the Tropic of Cancer at summer solstice. For the PS77-scheme, $d_e$ theoretically had a constant value of 105.9 m; thus, the difference ranged from 10 m to 35 m (9 - 33 % of 105.9 m).

Figure 6b shows the vertical structure of the effective vertical attenuation for the annual-mean radiation, defined in each 1m-layer and expressed by the e-folding depth $\zeta(\zeta(z) = 1/ln(I(z - 0.5)/I(z + 0.5)))$. The maximum vertical difference in $\zeta$ of about 1 m is seen in the upper 100 m layer at the equator, while $\zeta$ is almost vertically homogeneous at the high latitudes. The vertical structure originates from the diurnal and seasonal variations of the solar altitude. For PS77, $\zeta$ is a constant 23 m. Also shown in Fig. 6b are the annual-mean euphotic layer depths

for the PS77 (constant, 105.9 m) and IY10 (sinusoidal) schemes. The range of the latter (75 - 94 m) is somewhat narrower than that in Fig. 6a because of the annual averaging process.

Panels c and d of Fig. 6 show absorption of the annually averaged irradiance of the PS77 scheme expressed by its vertical convergence, and the difference in absorption between IY10 and PS77 (IY10-PS77), respectively. The absorption pattern naturally indicates latitudinal variation for both PS77 and IY10 (not shown for IY10), but the difference between the two hardly has any latitudinal variation (Fig. 6d), with the zero line staying at about 20 m at all latitudes. Introducing the solar altitude variation results in more warming at levels shallower than 20 m and more cooling below that level.
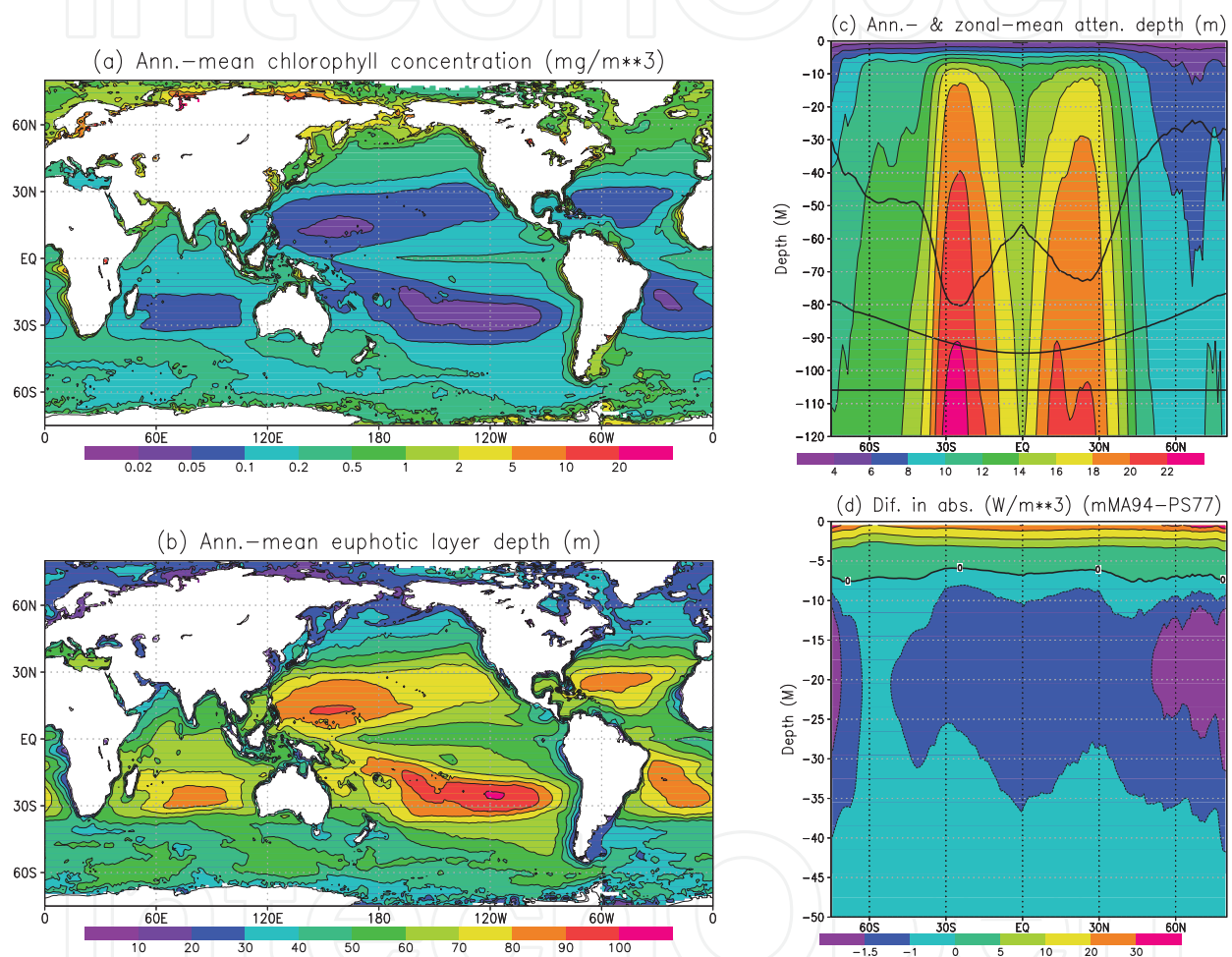


Fig. 7. (a) Annual-mean chlorophyll concentration (SeaWifs) [mg m$^{-3}$]. (b) Annual-mean euphotic layer depth [m] base on MA94 with diurnal variation of sun altitude (mMA94). (c) Effective attenuation depth $\zeta$ (m) for zonally averaged annual-mean penetrative irradiance of mMA94. (d) Difference in absorption between mMA94 and PS77 [W m$^{-3}$] (mMA94 - PS77). The thick lines in (c) indicate the zonally averaged annual-mean euphotic layer depth for mMA94 (uppermost), IY10 (middle) and PS77 (lowest, constantly 105.9 m).

### 3.3.2 Difference between mMA94 and PS77 schemes

Annual mean chlorophyll-a concentration (SeaWiFS) is shown in Fig. 7a, which was obtained by averaging its monthly mean values. The values are very low in the subtropical circulations

in both hemispheres. In contrast, high values are seen near the continental coasts. The corresponding annual mean euphotic layer depth based on the mMA94 scheme (7) (Fig. 7b) exhibits a pattern similar to that of chlorophyll-a. It has large values exceeding 80 m in the center of every subtropical circulation area, and exceeds 100 m in the South Pacific, which is greater than the largest value in IY10 (94 m, Fig. 6b). Very low values of less than 20 m are often observed along the continental coast, corresponding to high chlorophyll-a concentrations. Along the equator chlorophyll-a is relatively high and the euphotic layer depth is relatively shallow (50 - 60 m).

The effective attenuation depth calculated based on zonally averaged annual-mean penetrating irradiance is presented in Fig. 7c, with the zonal-mean euphotic layer depth for PS77, IY10, and mMA94. Figure 7d shows the difference in absorption between mMA94 and PS77 (mMA94 - PS77). In contrast with IY10, the effective attenuation depth (Fig. 7c) is very small (less than 8 m) in the top several-meter layer over the whole range of latitude. This is due to the fact that the attenuation depth $Z_1$ in the mMA94 scheme (7) is a few meters over the whole range of chlorophyll-a concentration. Corresponding to the low effective attenuation depth, the absorption is very large in the top layer in mMA94 compared to that in PS77 (Fig. 7d).

In the deeper layers below, 10 m, where the last term in (7) seems to be dominant, two peaks of dome-shaped distribution of high attenuation depth (low attenuation) correspond to the horizontal pattern of low chlorophyll-a and large euphotic layer depth (Figs. 7a and b). At the equator the two domes are divided, in contrast with IY10, where a single dome is centered at the equator (Fig. 6b). The high concentration of chlorophyll-a along the equator characterizes these optical properties and structures in the deeper part of the surface layer. The zonal-mean euphotic layer depth of mMA10 also has two peaks in magnitude, but much less than that of IY10 as a whole (Fig.7c). The zero line for the absorption difference (Fig. 7d) is at about 7 m over the whole range of latitude. Below that level, it has a vertical structure with a minimum in magnitude of 20 m, but its latitudinal variation seems to be very weak. The magnitude in the absorption difference for (mMA94 - PS77) is one order greater than that for (IY10 - PS77) (Fig. 6d).

## 3.4 Model and experiments

The OGCM used in this section is MRI.COM3 (Tsujino et al., 2010) that is, a free-surface, depth-coordinate ocean ice model. The model has a global domain with a tripolar grid (Murray, 1996) that consists of a spherical, latitude-longitude grid south of 64°N and a bipolar grid with generalized orthogonal coordinates with polar singularities in Siberia (64°N, 80°E) and Canada (64°N, 100°W).

The horizontal resolution is 1° in longitude and 0.5° in latitude south of 64°N. There are 50 vertical levels with a bottom boundary layer (Nakano & Suginohara, 2002). The surface layer thickness is 4 m, and the model has 30 levels in the upper 1000 m.

The mixed layer scheme is based on Noh & Kim (1999). The generalized Arakawa scheme (Ishizaki & Motoi, 1999) was used to calculate the momentum advection terms. A numerical advections scheme based on conservation of second-order moments (SOM) (Prather, 1986) was used for advection of tracers. Isopycnal diffusion (Redi, 1982) and eddy-induced transport parameterized as isopycnals layer thickness diffusion (Gent & McWilliams, 1990) are used as sub-grid-scale mixing.

The surface boundary conditions are based on the surface atmospheric condition by Large & Yeager (2009) and provided as the Coordinate Ocean-ice Reference Experiment (CORE) forcing dataset (CORE.v2). A detrended 59-year interannual forcing dataset from 1948 to 2006 was used for spin-up. More details about the model settings may be found in Tsujino et al. (2011).

The model was integrated for about 1,350 years (23 cycles) from an initial state by using the detrended CORE data, and reached a quasi-steady state. In the spin-up period, we used the PS77 scheme as the absorption scheme of solar radiation.

Three experiments were then carried out to examine the impact of the three absorption schemes described in the previous subsection. The first experiment used the conventional PS77 scheme and was called "CTL". The second experiment used the IY10 scheme and was called "SLR". The third experiment used the chlorophyll-a dependent scheme based on mMA94 scheme and was called "CHL". In the third experiment, chlorophyll-a data was derived from the monthly mean satellite-based observation (SeaWiFS: Fig. 7a). Each experiment started from a quasi-steady state and was integrated for five additional cycles (295 years) using the detrended CORE data. The yearly mean data over the fifth cycle were used for analysis.

### 3.5 Results

This subsection describes the impact of the three absorption schemes on ocean simulations. In particular, we focus on the oceanic structures of the tropical Pacific, where the impact of those schemes is most clearly found.

Figure 8a shows the SST and surface current differences between SLR and CTL. When the IY10 scheme was introduced, the SST increased slightly to about 0.1°C in the western tropical Pacific, the Indian Ocean and the subtropics. In contrast, the SST decreased to about 0.3°C in the central and eastern equatorial Pacific east of 175°E within the north-south 5 degrees band, together with the coastal areas. This SST contrast in the tropical Pacific Ocean has already been reported by IY10. Introducing the solar angle shifted the locus of radiation absorption upward, resulting in warming in the SST in all regions, except the eastern equatorial Pacific, where the indirect effect led to the cooling in the SST. When the mMY94 scheme was introduced (Fig. 8c), the pattern of the SST contrast in the tropical Pacific was almost the same, but the magnitude increased. The SST decreased in the eastern equatorial Pacific reaching even about 1°C around 120°W. The impact of the chlorophyll-a concentration (CHL) on the SST in the equatorial Pacific was about three times greater than that of the solar angle (SLR).

The IY10 scheme caused the westward current surface anomalies in the equatorial Pacific (Fig. 8a). The direction of the surface current anomalies turned pole ward apart from the equatorial region, corresponding to a divergent flow. This result is consistent with the impact of the IY10 scheme as described by IY10. These surface current anomalies are associated with increased upwelling and changes in the equatorial current system. Introduction of the chlorophyll-a concentration (CHL) produced effects similar to those of SLR, but with greater amplitude of the current anomaly (Fig. 8b). The amplitude is almost twice that of SLR, and the direction of the surface current is more pole ward. Thus, the divergent flow in the eastern equatorial Pacific is more enhanced in the CHL run than in the SLR run.
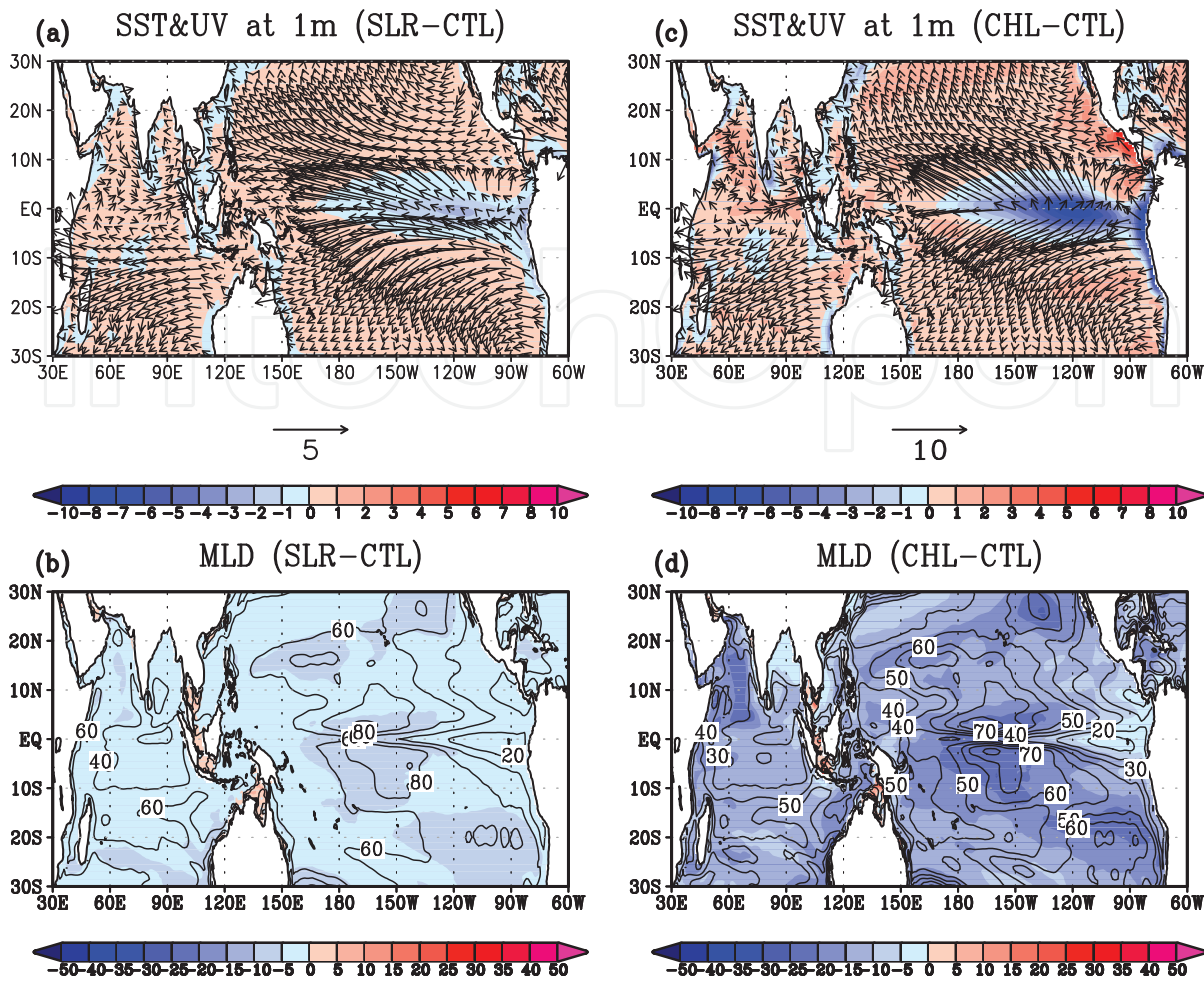
Fig. 8. (a) SST [0.1°C] (color) and surface current [cm/s] (vector) differences between SLR and CTL. (b) Mixed layer depth [m] difference between SLR and CTL (shaded) and mixed layer depth [m] for SLR (contour) . (c)-(d) Same as (a)-(b) but for CHL.

Introduction of the solar angle changed the vertical profile heating, due to solar radiation. The surface layer received more heating, while the subsurface layer received less (Fig. 6d, Fig. 7d). This vertical contrast of heating made the MLD shallower, over most regions (Fig. 8c). In the tropical Pacific, the MLD decreased to about 5 m in the central equatorial Pacific where the mean MLD was large. This situation was strengthened when the mMA94 scheme was used (Fig. 8d). Introducing the chlorophyll-a concentration made the MLD more than 20 m shallower. High chlorophyll-a concentration along the equator characterizes optical properties and structures in the deeper part of the surface layer, as mentioned in 3.3.2. The decrease in the MLD was also significant in the Arabian Sea, where chlorophyll-a concentration was relatively high (Fig. 7a). These changes in the MLD reflected the absorption differences among the mMA94, IY10, and PS77 schemes (Fig. 7d).

Changes in SSTs and surface currents of the equatorial Pacific due to the ocean radiant schemes were associated with a change in the shallow meridional circulation of the tropical Pacific, called the subtropical cell (STC). The STC played an important role in connecting subduction regions of the subtropical gyre with upwelling regions in the tropics. When the solar angle was introduced (Fig. 9a), the pole ward surface current in the upper 30 m, and
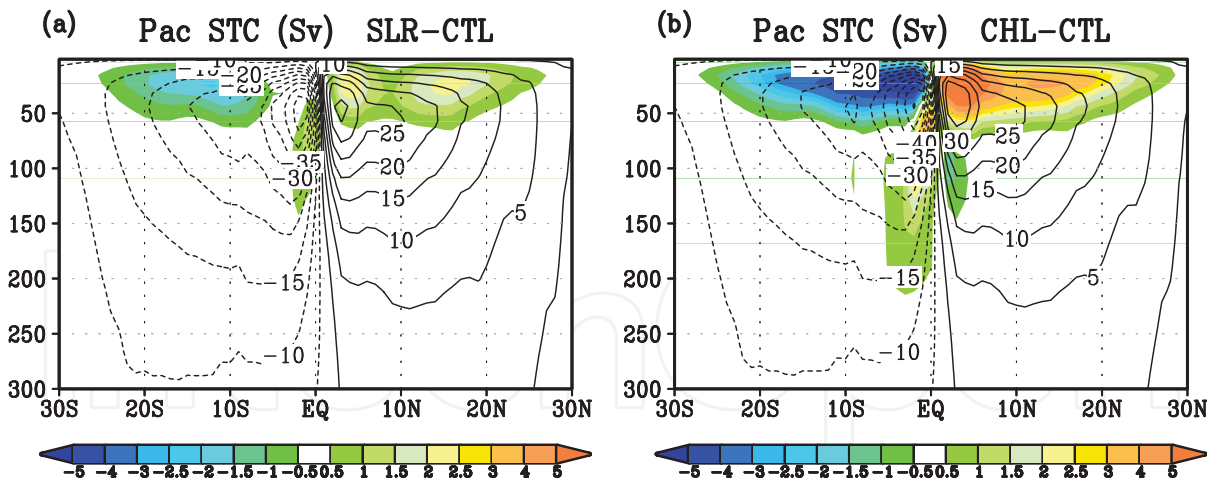
Fig. 9. (a) Meridional mass transport [Sv] zonally averaged in the Pacific Ocean for SLR (contour). The shaded area denotes the difference between SLR and CTL. (b) Same as (a) but for CHL.

the equator ward surface current at depths of 30 to 60 m were enhanced. This results in enhanced meridional circulation up to about 2.5 Sv (1Sv=$10^6$ m$^3$/s) in the North Pacific. Since the maximum transport of the STC is about 35 Sv in the mean state, the STC was strengthened by about 7 %. When the effect of chlorophyll-a concentration was introduced (Fig. 9b), similar current changes occured in the upper 70 m; however, the STC was further enhanced by about 7 Sv, corresponding to more than 20 % of the mean state. Thus, a more advanced ocean radiant scheme leads to more enhanced STC.

These results are understood from the following. In the tropical Pacific, the upper meridional transport ($M_y$) is expressed as (Sweeney et al., 2005):

$$M_y = \int_{D_{ML}}^{\eta} -\frac{1}{\rho_0 f}\frac{\partial p}{\partial x}dz + \frac{\tau_x}{\rho_0 f} \tag{8}$$

where $f$ is a Coriolis parameter, $\tau_x$ is a zonal wind stress, $\partial p/\partial x$ is a zonal pressure gradient, $\rho_0$ is sea water density, $\eta$ is a surface elevation, and $D_{ML}$ is a MLD. This equation means that the upper meridional transport is given by the difference between the pole ward Ekman transport and the equatorward geostrophic transport. The MLD is reduced by the introduction of the solar angle, or the effect of the chlorophyll-a distribution. The Ekman transport is the same in the three runs, because the employed surface wind stress is the same. Also, the difference between zonal pressure gradients in each run is small (Sweeney et al., 2005). Hence, the decreased MLD leads to the reduced meridional geostrophic transport. As a result, the pole ward transport increases, leading to an enhanced STC. The enhanced STC produces a divergent flow at the surface and strengthens the equatorial upwelling, and the resulting cold water from the deep layer cools the SST in the eastern equatorial Pacific.

To summarize, the impact of the changes in absorption schemes of the solar radiation on the tropical Pacific occurs not only due to the local heating of the solar radiation itself as a direct effect, but also by the dynamical response as an indirect effect. Introducing the chlorophyll-a distribution and varying the solar angle enhances the shallow meridional circulation (STC), which leads to nontrivial changes in the tropical oceanic structure.

## 4. Summary

This article examined the impact of solar radiation data and its absorption schemes on ocean model simulation. Both are essential for modeling the upper ocean thermal structure.

Section 2 investigated the discrepancy between observed and OGCM-simulated anomalies in recent SSTs of the tropical Indian Ocean. Observed SSTs indicate warming beginning in the late 1990s, whereas simulated SSTs exhibit cooling over the same period. Examination of surface heat fluxes in the OGCM showed that the simulated SST cooling was caused primarily by a decreasing trend in the reanalyzed solar radiation used as the surface boundary condition. In the atmospheric reanalysis, the decrease in solar radiation was attributed to an increase in cloud cover, deduced from precipitation data, and in part, responsible for the observed local warming of the Indian Ocean SSTs prescribed as the lower boundary condition. Observation-based estimates of precipitation, however, showed no significant increasing trend; thus, no increase in cloud cover was indicated. Caution is necessary when atmospheric reanalysis data are used for surface boundary conditions for OGCMs.

Section 3 examined three absorption schemes for ocean model simulations: (1) a conventional scheme (Paulson & Simpson, 1977), (2) an introduction of varying solar angle (Ishizaki & Yamanaka, 2010), and (3) an introduction of the effect of local heating by chlorophyll-a concentration (Morel & Antoine, 1994) together with the second scheme. Introducing the new scheme resulted in a significant change especially in the equatorial Pacific, where the MLD decreased by about 10 m, and the surface current field showed a divergent flow. Associated with the surface current field, the equatorial upwelling was enhanced and the STC transport intensifies by more than 20 % in the Pacific. These changes in SLR run are explained by a dynamical response of the equatorial Pacific to the change in MLD (Sweeney et al., 2005).

These results indicate that both the solar radiation data and the employed absorption scheme of solar radiation were important, especially in the tropical ocean. Careful attention must be paid to the treatment of solar radiation data and the absorption scheme of radiation for ocean modeling.

Further observation-based studies are needed to clarify the long-term trend of precipitation in the Indian Ocean. In addition, from the standpoint of ocean modeling, further progress on reanalysis products is desired to improve sea surface fluxes, for example by including air-sea interaction processes (e.g., Fujii et al., 2009), which are lacking in the current atmospheric reanalyses.

Although this study set the ratio of the longer-wavelength (IR) to the total at the surface to a constant ($R$ in (1)), atmospheric models generally treat direct rays and scattered light separately, and provide spectral intensities of radiation. Thus, the absorption of radiation in the sea can be accurately calculated by using coupled models. This is the next step of this study.

## 5. Acknowledgements

## 6. References

Adler, R. F.; Huffman G. J.; Chang, A.; Ferraro, R.; Xie, P.; Janowiak, J.; Rudolf, B.; Schneider, U.; Curtis, S.; Bolvin, D.; Gruber, A.; Susskind, J. & Arkin, P. (2003). The Version 2 Global Precipitation Climatology Project (GPCP) Monthly Precipitation Analysis (1979-Present). *J. Hydrometeor.*, Vol. 4, 1147-1167.

Anderson, W. G.; Gnanadesikan, A.; Hallberg, R.; Dunne, J. & Samuels, B. L. (2007). Impact of ocean color on the maintenance of the Pacific Cold Tongue. *Geophys. Res. Lett.*, Vol. 34, L11609, doi:1029/2007GL030100.

Arakawa, O. & Kitoh, A. (2004). Comparison of local precipitation-SST relationship between the observation and a reanalysis dataset. *Geophys. Res. Lett.*, Vol. 31, L12206, doi:10.1029/2004GL020283.

Copsey, D.; Sutton, R. & Knight, J. (2006). Recent trends in sea level pressure in the Indian Ocean region. *Geophys. Res. Lett.*, Vol. 31, L12206, doi:10.1029/2004GL020283.

Dee, D.; Uppala, S.; Kobayashi, S.; Lindskog, M. & Simmons, A. (2008). Developments in bias correction for reanalysis. *Proceedings of the 3rd WCRP International Conference on Reanalysis*, p58.

Deser, C. & Phillips, A. (2006). Simulation of the 1976/77 climate transition over the North Pacific: Sensitivity to tropical forcing. *J. Clim.*, Vol. 19, 6170-6180.

Du, Y.; Qu, T.; Meyer, G.; Masumoto, Y. & Sasaki, H. (2005). Seasonal heat budget in the mixed layer of the southeastern tropical Indian Ocean in a high-resolution ocean general circulation model. *J. Clim.*, Vol. 110, C04012, doi:10.1029/2004JC002845.

Fujii, Y.; Nakaegawa, T.; Matsumoto, S.; Yasuda, T.; Yamanaka, G. & Kamachi, M. (2009). Coupled climate simulation by constraining ocean fields in a coupled model with ocean data. *J. Clim.*, Vol. 22, No. 20, 5541-5557.

Gent, P. R. & McWilliams, J. C. (1990). Isopycnal mixing in ocean circulation model. *J. Phys. Oceanogr.*, Vol. 20, 150-155.

Gnanadesikan, A. & Anderson, W. G. (2009). Ocean water clarity and the ocean general circulation in a coupled climate model. *J. Phys. Oceanogr.*, Vol. 39, doi:10.1175/2008JPO3935.1, 314-332.

Han, W.; Meehl, G. & Hu, A. (2006). Interpretation of tropical thermocline cooling in the Indian and Pacific oceans during recent decades. *Geophys. Res. Lett.*, Vol. 33, L23615, doi:10.1029/2006GL027982.

Hoerling, M. P.; Hurrell, J. W.; Xu, T.; Bates, G. T. & Phillips, A. S. (2004). Twentieth century North Atlantic climate change: Part II. Understanding the effect of Indian Ocean warming. *Clim. Dyn.*, Vol. 23, No. 3-4, 391-405.

Ishii, M.; Shoji, A.; Sugimoto, S. & Matsumoto, T. (2005). Objective Analyses of SST and marine meteorological variables for the 20th Century using ICOADS and the Kobe Collection. *Int. J. Climatol.*, Vol. 25, 865-879.

Ishikawa, I.; Tsujino, H.; Hirabara, M.; Nakano, H.; Yasuda T. & Ishizaki, H. (2005). Meteorological Research Institute Community Ocean Model (MRI.COM) Manual. (in Japanese). *Technical reports of the Meteorological Research Institute*, Vol. 47, 1-189.

Ishizaki, H. & Motoi, T. (1999). Reevaluation of the Takano-Onishi scheme for momentum advection on bottom relief in ocean models. *J. Atmos. Ocean Technol.*, Vol. 16, 1994-2010.

Ishizaki, H. & Yamanaka, G. (2010). Impact of explicit sun altitude in solar radiation on an ocean model simulation. *Ocean Modelling*, Vol. 33, 52-69.

Jerlov, N. G. (1968). *Optical Oceanography*, Elsevier, pp. 194.

Kalnay, E.; Kanamitsu, M.; Kistler, R.; Collins, W.; Deaven, D.; Gandin, L.; Iredell, M.; Saha, S.; White, G.; Woollen, J.; Zhu, Y.; Chelliah, M.; Ebisuzaki, W.; Higgins, W.; Janowiak, J.; Mo, K. C.; Ropelewski, C.; Wang, J.; Leetmaa, A.; Reynolds, R.; Jenne, R. & Joseph, D. (1996). The NCEP/NCAR 40-years reanalysis project. *Bull. Am. Meterol. Soc.*, Vol. 77, 437-471.

Kanamitsu, M.; Ebisuzaki, W.; Woolen, J.; Yang, S-K.; Hnilo, J. J.; Fiorino, M. & Potter, G. L. (2002). NCEP-DOE AMIP-II reanalysis (R-2). *Bull. Am. Meterol. Soc.*, Vol. 83, 1631-1643.

Kara, A. B.; Rochford, P. A.; & Hulburt, H. E. (2000). Efficient and accurate bulk parameterizations of air-sea fluxes for use in general circulation models. *J. Atmos. Ocean Technol.*, Vol. 17, 1421-1438.

Large, W. G. & Yeager, S. G. (2004). Diurnal to decadal global forcing for ocean and sea-ice models: the data sets and flux climatologies. *NCAR Technical Note*, NCAR/TN-460+STR.

Large, W. G., & Yeager, S. G., (2009). The global climatology of an interannualy varying air sea flux data set. *Clim. Dyn.*, Vol. 33, 341-363. doi:10.1007/s00382-008-0441-3.

Lau, K. M. & Weng, H. Y. (1999). Interannual, decadal-interdecadal, and global warming signals in sea surface temperature during 1955-97. *J. Clim.*, Vol. 12, No. 5, 1257-1267.

Levitus, S.; Antonov, J. & Boyer, T. (2005). Warming of the world ocean, 1955-2003. *Geophys. Res. Lett.*, Vol. 32, L02604, doi:10.1029/2004GL021592.

Manizza, M.; Quere, C. L.; Watson, A. J. & Buitenhuis, E. T. (2005). Bio-optical feedbacks among phytoplankton, upper ocean physics and sea-ice in a global model. *Geophys. Res. Lett.*, Vol. 32, L05603.

Morel, A. (1988). Optical modeling of the upper ocean in relation to its biogenous matter content (Case I waters). *J. Geophys. Res.*, Vol. 93, 10749-10768.

Morel, A. H. & Antoine, D. (1994). Heating rate within the upper ocean in relations to its biooptical state. *J. Phys. Oceanogr.*, Vol. 24, 1652-1665.

Morel, A. H. & Berthon, J. F. (1989). Surface pigments, algal biomass profiles, and potential production of the euphotic layer: Relationships reinvestigated in view of remote sensing applications. *Limnol. Oceanogr.*, Vol. 34, No. 8, 1545-1562.

Morel, A. H. & Prieur, L. (1977). Analysis of variations in ocean color. *Limnol. Oceanogr.*, Vol. 22, 709-722.

Murray, R. J. (1996). Explicit generation of orthogonal grids for ocean models. *J. Comput. Phys.*, Vol. 126, 251-273.

Murtugudde, R. & Busalacchi, A. J. (1999). Interannual variability of the dynamics and thermodynamics of the tropical Indian Ocean. *J. Clim.*, Vol. 12, 2300-2326.

Murtugudde, R.; Beauchamp, J.; McClain, C. R.; Lewis, M. & Busalacchi, A. J. (2002). Effects of penetrative radiation on the upper tropical ocean circulation. *J. Clim.*, Vol. 15, 470-486.

Nakamoto, S.; Kumar, S.; Oberhuber, J.; Ishizaka, J.; Muneyama, K. & Frouin, R. (2001). Response of the equatorial Pacific to chlorophyll pigment in a mixed layer isopycnal ocean general circulation model. *Geophys. Res. Lett.*, Vol. 28, 2021-2024.

Nakano, H. & Suginohara, N. (2002). Effects of bottom boundary layer parameterization on reproducing deep and bottom waters in a world ocean model. *J. Phys. Oceanogr.*, Vol. 32, 1209-1227.

Noh, Y. & Kim, H-J. (1999). Simulations of temperature and turbulence structure of the oceanic boundary layer with the improved near-surface process. *J. Geophys. Res.*, Vol. 104, 15621-15634.

Norris, J. R. (2005). Trends in upper-level cloud cover and surface divergence over the tropical Indo-Pacific Ocean between 1952 and 1997. *J. Geophys. Res.*, Vol. 110, D21110, doi:10.1029/2005JD006183.

Ohlmann, J. C. (2003). Ocean radiant heating in climate models. *J. Clim.*, Vol. 16, 1337-1351.

Ohlmann, J. C.; Siegel, D. A. & Mobley, C. D. (2000). Ocean radiant heating. Part I: Optical influences. *J. Phys. Oceanogr.*, Vol. 30, 1833-1848.

Ohlmann, J. C. & Siegel, D. A. (2000). Ocean radiant heating. Part II: Parameterizing solar radiation transmission through the upper ocean. *J. Phys. Oceanogr.*, Vol. 30, 1833-1848.

Onogi, K.; Tsutsui, J.; Koide, H.; Sakamoto, M.; Kobayashi, S.; Hatsushika, H.; Matsumoto, T.; Yamazaki, N.; Kamahori, H.; Takahashi, K.; Kadokura, S.; Wada, K.; Kato, K.; Oyama, R.; Ose, T.; Mannoji, N. & Taira, R. (2007). The JRA-25 reanalysis. *J. Meteor. Soc. Japan*, Vol. 85, 369-432.

Paulson, C. & Simpson, J. (1977). Irradiance measurements in the upper ocean. *J. Phys. Oceanogr.*, Vol. 7, 952-956.

Prather, M. J. (1986), Numerical advection by conservation of second-order moments. *J. Geophys. Res.*, Vol. 91, 6671-6681.

Redi, M. H. (1982), Oceanic isopycnals mixing by coordinate rotation. *J. Phys. Oceanogr.*, Vol. 12, 1154-1158.

Sweeney, C.; Gnanadesikan, A.; Griffies, S. M.; Harrison, M. J.; Rosati, A. J. & Samels, B. L. (2005). Impacts of shortwave penetration depth on large-scale ocean circulation and heat transport. *J. Phys. Oceanogr.*, Vol. 35, 1103-1119.

Tsujino, H.; Motoi, T.; Ishikawa, I.; Hirabara, M.; Nakano, H.; Yamanaka, G.; Yasuda, T. & Ishizaki, H. (2010). Reference manual for the Meteorological Research Institute Community Ocean Model (MRI.COM) version 3. *Technical reports of the Meteorological Research Institute*, Vol. 59, 1-241.

Tsujino, H.; Hirabara, M.; Nakano, H.; Yasuda, T.; Motoi, T. & Yamanaka, G. (2011). Simulating present climate of the global ocean-ice system using the Meteorological Research Institute Community Ocean Model (MRI.COM): simulation characteristics and variability in the Pacific sector. *J. Oceanogr.*, Vol. 67, 449-479. doi:10.1007/s10872-011-0050-3.

Tsutsui, J. & Kadokura, S. (2008). Multiple regression analysis of the JRA-25 monthly temperature. *Proceedings of the 3rd WCRP International Conference on Reanalysis*, pp. 28.

Uppala, S. M.; Kållberg, P. W.; Simmons, A. J.; Andrae, U.; da Costa Bechtold, V.; Fiorino, M.; Gibson, J. K.; Haseler, J.; Hernandez, A.; Kelly, G. A.; Li, X.; Onogi, K.; Saarinen, S.; Sokka, N.; Allan, R. P.; Andersson, E.; Arpe, K.; Balmaseda, M. A.; Beljaars, A. C. M.; van de Berg, L.; Bidlot, J.; Bormann, N.; Caires, S.; Chevallier, F.; Dethof, A.; Dragosavac, M.; Fisher, M.; Fuentes, M.; Hagemann, S.; Hólm, E.; Hoskins, B. J.; Isaksen, L.; Janssen, P. A. E. M.; Jenne, R.; McNally, A. P.; Mahfouf, J-F.; Morcrette, J-J.; Rayner, N. A.; Saunders, R. W.; Simon, P.; Sterl, A.; Trenberth, K. E.; Untch, A.; Vasiljevic, D.; Viterbo, P. & Woollen, J. (2005). The ERA-40 re-analysis. *Quart. J. Roy. Meteor. Soc.*, Vol. 131, 2961-3012.

Wang, B.; Wu R. & Fu, X. (2000). Pacific-East Asian teleconnection: How does ENSO affect East Asian climate ? *J. Clim.*, Vol. 13, 1517-1536.

Watanabe, M. & Jin, F.-F. (2002). Role of Indian Ocean warming in the development of Philippine Sea anticyclone during ENSO. *Geophys. Res. Lett.*, Vol. 29, 1478, doi:10.1029/2001GL014318.

Xie, P. & Arkin, P. (1996). Analysis of global monthly precipitation using gauge observations, satellite estimates, and numerical model predictions. *J. Clim.*, Vol. 9, 840-858.

Yamanaka, G. (2008). Discrepancies between observed and ocean general circulation model-simulated anomalies in recent SSTs of the tropical Indian Ocean caused by apparent trends in atmospheric reanalysis data. *Geophys. Res. Lett.*, Vol. 35, doi:10.1029/2008GL034737.
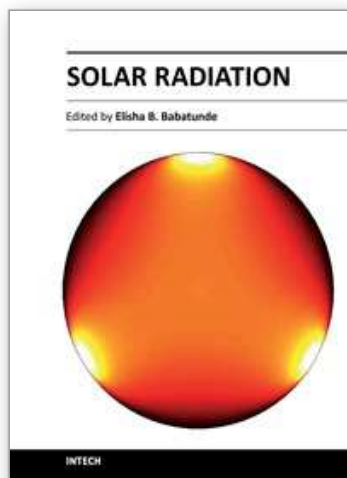
**Solar Radiation**

Edited by Prof. Elisha B. Babatunde

The book contains fundamentals of solar radiation, its ecological impacts, applications, especially in agriculture, architecture, thermal and electric energy. Chapters are written by numerous experienced scientists in the field from various parts of the world. Apart from chapter one which is the introductory chapter of the book, that gives a general topic insight of the book, there are 24 more chapters that cover various fields of solar radiation. These fields include: Measurements and Analysis of Solar Radiation, Agricultural Application / Bio-effect, Architectural Application, Electricity Generation Application and Thermal Energy Application. This book aims to provide a clear scientific insight on Solar Radiation to scientist and students.

**How to reference**

In order to correctly reference this scholarly work, feel free to copy and paste the following:

Goro Yamanaka, Hiroshi Ishizaki, Hiroyuki Tsujino, Hideyuki Nakano and Mikitoshi Hirabara (2012). Impact of Solar Radiation Data and Its Absorption Schemes on Ocean Model Simulations, Solar Radiation, Prof. Elisha B. Babatunde (Ed.), ISBN: 978-953-51-0384-4, InTech, Available from:
http://www.intechopen.com/books/solar-radiation/impact-of-solar-radiation-data-and-its-absorption-schemes-on-ocean-model-simulations

# INTECH
open science | open minds